

Torque allocation of four-wheel drive EVs considering tire slip energy

Bingzhao GAO¹, Yongjun YAN¹, Hong CHU¹, Hong CHEN^{2,1} & Nan XU^{1*}¹State Key Laboratory of Automotive Simulation and Control, Jilin University, Changchun 130025, China;²Clear Energy Automotive Engineering Center, Tongji University, Shanghai 201804, China

Received 27 December 2019/Revised 16 March 2020/Accepted 30 April 2020/Published online 18 May 2021

Abstract With the increasing peak torque of the in-wheel motor, the tire slip energy dissipation becomes as considerable as the motor energy loss. The actuation redundancy in four-wheel drive electric vehicles has the innate advantage of reducing the energy dissipation of the tire slip according to different criteria. This study innovatively optimizes the energy loss of the motor and the slip energy consumption of the tire under a unified framework. A more accurate calculation model of the tire slip force and slip energy is adopted in the cost function. Its feasibility and potential are shown through simulation case studies based on different road adhesion coefficients among three allocation methods: considering both motor energy loss and tire slip loss, only considering the motor energy loss, and only considering the axis load distribution. The simulation results demonstrate that the torque allocation method considering both motor energy loss and tire slip loss can dramatically reduce the tire slip energy and tire wear with an acceptable motor energy efficiency sacrifice compared to the present allocation algorithms.

Keywords control allocation, four-wheel drive electric vehicles, tire slip energy model, multi-objective optimization

Citation Gao B Z, Yan Y J, Chu H, et al. Torque allocation of four-wheel drive EVs considering tire slip energy. *Sci China Inf Sci*, 2022, 65(2): 122202, <https://doi.org/10.1007/s11432-019-2946-8>

1 Introduction

At present, range anxiety is a major obstacle for electric vehicles in terms of further increasing their market share. The conventional methods for solving this problem include the lightweight design of the body structure, high-capacity energy storage devices, and vehicle aerodynamic shape optimization. For four-wheel drive electric vehicles (4WD EVs), their unique power transmission mode brings the advantages of high transmission efficiency, rapid power response speed, and high power response precision. However, an actuation redundancy is obtained because of the existence of multiple power sources. The appropriate torque distribution will improve not only the vehicle's steering stability, but, more importantly, its energy efficiency [1].

The torque allocation objective must consider many factors, and powertrain efficiency is one of them. For 4WD EVs, the required torque must be distributed according to the motor efficiency to achieve an optimized speed. The majority of existing control strategies centralize most or all of the torque load on the front or rear axles to improve the efficiency of the whole vehicle when the total torque demand is small [2]. A hierarchical control structure was proposed in [3], where the high-level dynamic sliding mode control aimed to track the planar motions, and the low-level adaptive energy-efficient control allocation was constituted to optimize energy consumption considering the in-wheel/hub motor torque distribution. Discarding complex algorithms, Ref. [1] presented a fast and feasible torque distribution strategy based on the hypothesis of the powertrain loss function. The results obtained confirmed the validity of the proposed control allocation algorithm in [2–4].

Note that several power loss sources are considered during the operation of 4WD EVs. In particular, the power dissipation caused by tire slip is intensely influenced by the control allocation [5]. Compared to

* Corresponding author (email: xu.nan0612@gmail.com)

conventional internal combustion engine vehicles, 4WD EVs have a higher power output and a more rapid torque response, making the slip ratio control more significant [6]. Some researchers have proposed various ingenious control methods (e.g., model predictive control [7, 8], feedforward and feedback control [9], and sliding mode control [10]) to control the tire slip rate to follow the optimal slip rate value or remain within the appropriate slip rate range under current parameters. Aside from this, the vertical load is another tire force distribution principle. The results in [11] implied that the performance in vehicle lateral stability and maneuverability can be significantly improved using the tire dynamic load-based torque distribution algorithm with longitudinal and lateral slip constraints. A similar conclusion can be found in [12], which presented an adaptive nonlinear control scheme aiming to improve the handling properties of vehicles. A main loop and eight cascade loops are the basic components of the integrated control system. Overall, the original intention of these methods is to optimize torque distribution of torque from the aspect of vehicle stability. Energy saving has not been explicitly considered.

Additionally, the energy loss ratio-based driving force distribution of independent four-wheel drive vehicles is more efficient for vehicles moving on a rigid ground than the tire workload-based distribution strategy [13, 14]. To a certain extent, energy-based criteria facilitate handling stability [15]. The above-mentioned tire energy loss models were based on tire force and tire slip velocity. However, the tire contact patch contains adhesion and slip region; hence, using the slip force in the contact patch is more direct and effective for obtaining the tire slip energy [16]. Accordingly, for this problem, an online estimation model of the tire energy dissipation was proposed by [17] using a brush tire model. In this case, the slip force can be accurately calculated in the slip region. A more reasonable torque distribution method considering the tire slip energy consumption was proposed in [16, 18]. Their result proved that slip energy reduction can improve stability and durability under extreme conditions with an obvious economic benefit [19, 20]. The hierarchical controller is another promising tool for considering the tire energy dissipation at a lower level [21, 22]. Previous evidence shows that the tire slip energy seems isolated from other vehicle energy losses (e.g., motor loss energy). Hence, the feasibility of the torque allocation method must be tested while considering motor loss and tire slip energy at the same time.

In summary, this study aims to construct a reasonable torque allocation method considering both motor power loss and tire slip energy dissipation, which indicates tire wear, at a unified scale. A concentrated control structure that regards the front and rear wheel torques as independent control variables is applied. Moreover, we look forward to reducing the tire slip energy and the tire wear dramatically with an acceptable motor energy efficiency sacrifice. A more precise tire slip energy model is used to characterize the slip dissipation. The simulation result shows a noteworthy improvement in the energy efficiency compared with that of two other torque allocation methods under a road with different adhesion coefficients.

The remainder of this paper is organized as follows: Section 2 discusses the vehicle and tire modeling used to construct the optimal problem formulation of the wheel torque allocation algorithm; Section 3 describes the cost function, inequality constraint, and boundary condition of the optimal problem; Section 4 presents the algorithm for solving the torque allocation optimization problem; Section 5 demonstrates the effectiveness of the proposed economic-oriented wheel torque allocation strategy compared with the other two methods under different conditions through simulations; and finally, Section 6 provides the conclusions of this study.

2 Control-oriented system modeling

2.1 System description

The system analyzed herein is that of 4WD EVs. The wheels of the vehicle are directly connected to four external rotor hub motors (Figure 1); hence, devices (e.g., reducers or gearboxes) are no longer needed. This powertrain configuration will reduce efficiency degradation and leave space inside the vehicle to allow sufficient battery packs giving an adequate range. The energy management control unit can calculate the appropriate torque allocation among four in-wheel motors according to the feedback information, including battery state of charge, driving task, and tire-road friction forces [23]. Figure 1 presents the energy flow analysis during the acceleration condition of the 4WD EVs. As shown in the figure, most of the battery energy is converted to kinetic energy of the vehicle in the acceleration condition. Moreover, approximately 11% and 5% of the battery energy loss are caused by the motor core and tire

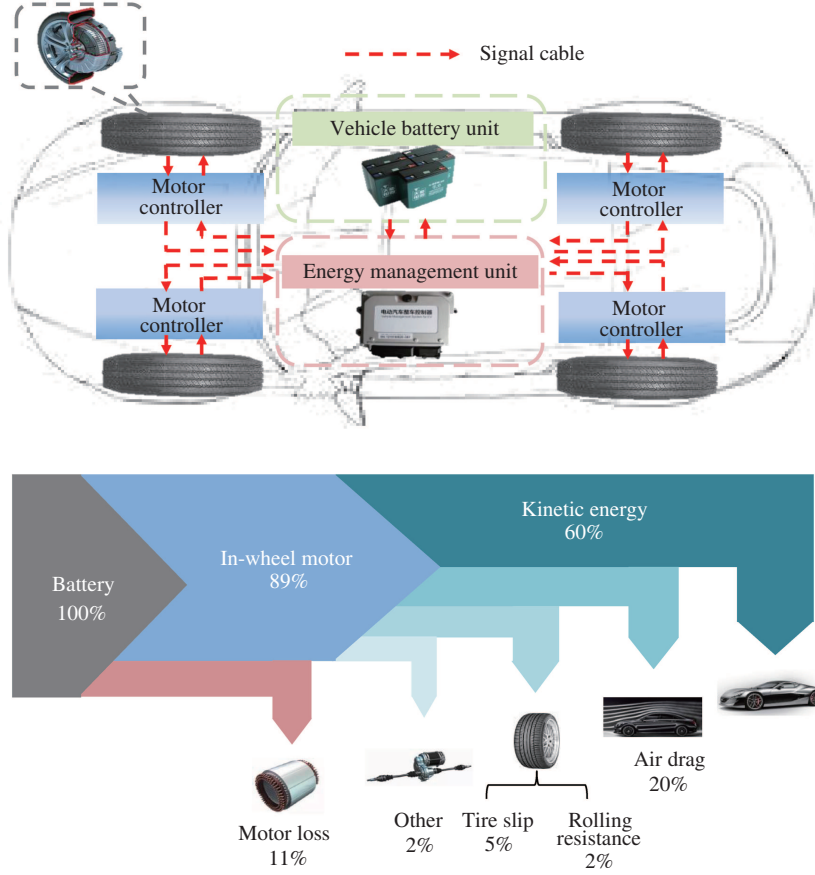


Figure 1 (Color online) System configuration and energy flow analysis of the four in-wheel motor drive EVs [5, 24].

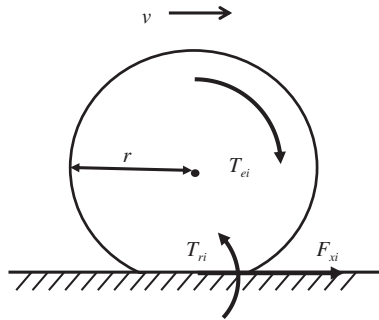


Figure 2 Force analysis of tire rotation, i stands for f (front wheel) or r (rear wheel) respectively.

slip, respectively. This result provides the fundamental mechanism of this study.

2.2 Vehicle model

Based on the research reviewed, this study hypothesizes that the power of the motor on the left side of the vehicle is always equal to that on the right side, which means that the proposed algorithm will optimize the torque of the front and rear wheels. Notably, the pitch and roll dynamics of the car body are not taken into account.

The equation of rotational motion of each wheel (as shown in Figure 2) can be described as

$$T_{ei} - T_{ri} - F_{xi} \cdot r - T_b = 0, \quad i = r, f, \tag{1}$$

where T_{ei} is the wheel drive torque, the assumption is made that there is no power loss from the motor to the wheel due to the advantage coming from the in-wheel motor, so the T_{ei} is approximately the same

as motor output torque. T_{ri} is the rolling resistance caused by tire's elastic hysteresis at the wheel i , F_{xi} is the longitudinal driving force at the wheel i , r represents the wheel radius, T_b is the brake torque. Different from other studies considering the handling stability of the vehicle, the tire moment of inertia is not considered when modeling the rotational force of the tire, the reason is that torque allocation for considering energy consumption is a long-term optimization problem. In this process, the value of the wheel inertia with hub motor is about $3 \text{ kg}\cdot\text{m}^2$, and the instantaneous change rate of wheel speed is marginal. Therefore, the moment of inertia can be relatively ignored.

Since the research topic is limited to the acceleration condition in this study, the braking torque can also be ignored, and the situation that the permanent magnet motors recapture braking energy in the battery in reverse is not considered. The above formula is converted to

$$F_{xi} = \frac{1}{r}T_{ei} - \frac{1}{r}T_{ri}, \quad i = r, f. \quad (2)$$

Based on the analysis of the vehicle body, the following equation can be obtained

$$2(F_{xr} + F_{xf}) = F_a + m \cdot \dot{v} + F_{\text{slop}}, \quad (3)$$

where m is the vehicle mass, v is the longitudinal vehicle speed, F_{slop} is the slop resistance, the air resistance F_a is as

$$F_a = \frac{1}{2}C_D A \rho \cdot v^2, \quad (4)$$

where C_D is the air resistance coefficient, A is the windward area, ρ is the air density.

From (1) and (3), the following equation is obtained

$$\dot{v} = \frac{2}{mr}(T_{er} + T_{ef}) - 2\mu g - \frac{1}{m}F_a - \frac{1}{m}F_{\text{slop}}, \quad (5)$$

where μ is the rolling resistance coefficient.

Because the acceleration generated during vehicle acceleration will cause load transfer, the vertical force of each tire of 4WD EVs is calculated as

$$F_{zf} = 0.5 \left(mg \frac{l_2}{l} \cos \theta - mg \frac{h_g}{l} \sin \theta - m \frac{h_g}{l} \dot{v} \right), \quad (6)$$

$$F_{zr} = 0.5 \left(mg \frac{l_1}{l} \cos \theta + mg \frac{h_g}{l} \sin \theta + m \frac{h_g}{l} \dot{v} \right), \quad (7)$$

where l_1 and l_2 are the distances of the front and rear axles from the vehicle center of gravity (CG), l is the wheelbase of the vehicle, m is the total mass of the vehicle, h_g is the height of the vehicle center of gravity, and g is the gravitational acceleration constant, θ is the road slope that is assumed to be zero in this study.

2.3 Tire model

When the longitudinal and the lateral forces of the tire are determined, the next step is to calculate the slip rate with tire inverse model. As for the tire inverse model, it should be able to reflect the nonlinear characteristics of the tire, with higher precision and simple form to carry out reversal derivation.

The Dugoff tire model [25] has high accuracy and can reflect the longitudinal slip characteristics delicately. It has few parameters and a simple structure. These characteristics enable it to meet the above needs. First, the tire slip rate is defined as

$$S_x = \frac{\omega r - v}{\max(\omega r, v)}, \quad (8)$$

where S_x is the longitudinal slip ratio, ω is the wheel rotation speed, r is the wheel radius, v is the longitudinal vehicle speed. Since the analysis is performed on a single wheel, the front and rear tires are no longer distinguished in the formula of this section, and the tire force and parameters will be uniformly stated. Then, the Dugoff tire model can be shown as

$$\begin{cases} F_x = C_\lambda \frac{S_x}{1 + S_x} f(H_D), \\ F_y = C_\alpha \frac{\tan \alpha}{1 + S_x} f(H_D), \end{cases} \quad (9)$$

$$f(H_D) = \begin{cases} (2 - H_D) H_D, & H_D < 1, \\ 1, & H_D \geq 1, \end{cases} \quad (10)$$

$$H_D = \frac{\mu_f F_z (1 + S_x)}{2\sqrt{(C_\lambda S_x)^2 + (C_\alpha \tan \alpha)^2}}, \quad (11)$$

where α is the wheel sideslip angle, C_λ is the longitudinal stiffness, C_α is the cornering stiffness. F_x, F_y, F_z are the longitudinal tire force, lateral tire force, and vertical tire force. To derive the slip rate of the tire from the tire force, we need to sort the above model to get the modified inverse tire model. Since the original Dugoff tire model contains two nonlinear switched algebraic equations, an intermediate variable D will be defined firstly, corresponding to the previous switching variable H_D , to make a judgment.

$$D = \frac{\mu_f F_z}{2\sqrt{F_x^2 + F_y^2}}. \quad (12)$$

If inequality ($D \geq 1$) is real, the modified inverse tire model is shown as

$$S_x = \frac{F_x}{C_\lambda - F_x}. \quad (13)$$

Conversely, if D is less than 1, the modified inverse tire model is shown as

$$S_x = \frac{\mu_f^2 F_x F_z^2}{4C_\lambda F_x (\mu_f F_z - F_x) - \mu_f^2 F_x F_z^2}. \quad (14)$$

Since this paper only focuses on the longitudinal force of the tire and the longitudinal slip caused by it, the lateral force and the side angle will be ignored in the tire model.

The slopes of the pure slip curves are defined as the longitudinal slip stiffness. The longitudinal slip stiffness is one of the most crucial property parameters of the tire and is crucial for the vehicle's handling and stability performance. According to [26], the longitudinal slip stiffness is (almost) linearly dependent on the vertical force for many tires. Regarding the magic formula, we can get the relationship between the vertical tire force and the longitudinal slip stiffness.

$$C_\lambda = k_s (C_a F_z^2 + C_b F_z) \exp(-C_c F_z), \quad (15)$$

where C_λ is the tire longitudinal slip stiffness, C_a, C_b, C_c, k_s are the fitting coefficients which fitted from actual tire test data.

The online estimation of the tire slip energy is essential to use tire slip energy as an optimization criterion. As energy dissipation rate due to tire slip is the multiplication of the slip speed and force, the energy dissipation rate cannot be directly described by the tire force commands [18]. The tire contact patch of a driving vehicle is divided as adhesion and sliding regions. In the adhesion region, the tire surface will undergo elastic deformation and make itself adhere to the ground, it will not produce slip energy in this region. So the cause of the tire slip energy is mainly contributed to the relative slip between the tire surface and the ground in the slip region of tire contact patch.

In Figure 3, XOY is a relative coordinate system for describing the tread deformation with respect to the carcass. The origin "O" is the contact patch center. "AB" is the adhesion region and "BC" is the sliding region, divided by the initial sliding point "B". After rolling for a period of time, a point in contact patch, which begins to contact at the point "A", is now reaching the position "P_t", the commensurate point on carcass moves to "P_c". As illustrated in the picture, the distance from "P_c" to coordinate origin x and the half length of contact patch a obeys the following equation $V_t t = a - x$, the longitudinal deformation of element is

$$\Delta x = (a - x) S_x. \quad (16)$$

The shear stresses of tread element in longitudinal directions can be expressed as

$$q_x = k_{tx} \cdot \Delta x = k_{tx} \cdot (a - x) S_x, \quad (17)$$

where k_{tx} is the stiffness of tread element in the longitudinal direction, $2a$ is the whole length of contact patch.

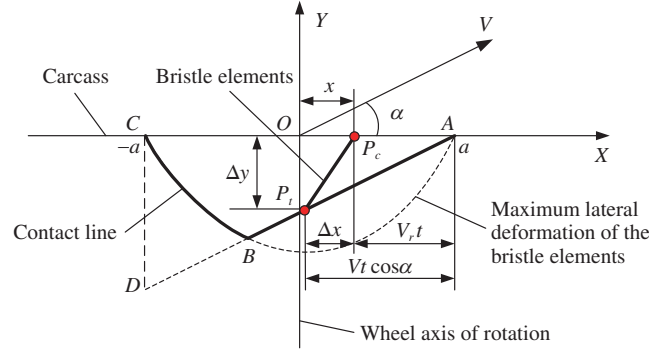


Figure 3 (Color online) Deformation of the bristles in the tire contact patch under combined slip conditions.

The deformation of tread element will be restrained by the maximum friction force over the contact patch, the initial sliding condition is

$$q(u_c) = \mu q_z = \frac{\mu F_z}{2a} \eta(u_c), \tag{18}$$

where μ is the directional friction coefficient, $\eta(u_c)$ is the pressure distribution function, $u_c = x_c/a$ is the relative coordinate of the initial sliding point.

The initial sliding condition can be converted to

$$\frac{\eta(u_c)}{1 - u_c} = \phi_x = \frac{K_x S_x}{\mu_x F_z} \quad (-1 \leq u_c \leq 1), \tag{19}$$

where ϕ_x represents the normalized longitudinal slip ratio, K_x represents the tire longitudinal slip stiffness, S_x represents the tire longitudinal slip ratio, μ_x is the longitudinal friction coefficient, F_z is the vertical tire force.

Accordingly, the total tangential force in the tire contact patch is

$$\begin{aligned} F &= \int_{x_c}^a q dx + \int_{-a}^{x_c} \mu \cdot \frac{F_z}{2a} \cdot \eta(u) dx \\ &= \frac{(1 - u_c)^2}{4} \cdot 2a^2 \sqrt{(k_{tx} S_x)^2 + (k_{ty} S_y)^2} + \mu F_z \cdot \frac{m_0(u_c)}{2}, \end{aligned} \tag{20}$$

where $m_0(u_c) = \int_{-1}^{u_c} \eta(u) du$ is the zero-order moment of $\eta(u)$ in the sliding regions.

From the equation above, we can get the expression of force in the sliding regions of tire contact patch F_s ,

$$F_s = \frac{\mu F_z}{2} \int_{-1}^{u_c} \eta(u) du. \tag{21}$$

In order to get the tire slip force, the initial sliding point and pressure distribution should be determined. In this paper, we use the parabolic pressure distribution which is proposed in [27], it has the following expression:

$$\eta(u) = \frac{3}{2} (1 - u^2). \tag{22}$$

According to the (19), the initial sliding point could be deduced as

$$u_c = \frac{2}{3} \phi - 1 = \xi, \tag{23}$$

where ϕ is equal to ϕ_x since the vehicle longitudinal characteristic is only considered in this study. Then, we reassign the value of u_c to ξ . Substituting (22) into (21), the slip force could be written as

$$F_s = \frac{1}{4} \mu F_z (2 + 3\xi - \xi^3). \tag{24}$$

Moreover, the longitudinal slip velocity is

$$v_s = \frac{S_x}{1 - S_x} v_{\max}, \tag{25}$$

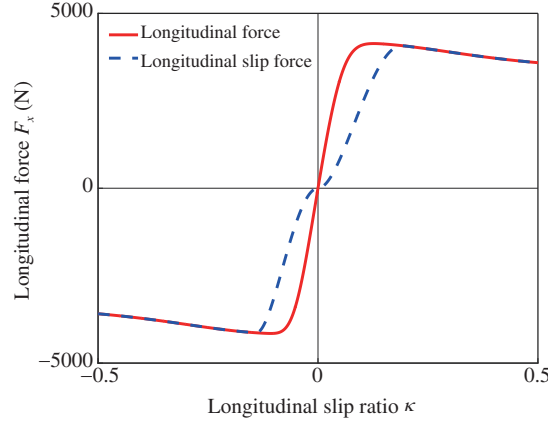


Figure 4 (Color online) Comparison between modified slip force and tire longitudinal force.

where v_{\max} represents the maximum of wheel velocity and v_s represents the vehicle longitudinal speed.

The tire slip energy can be obtained as

$$P_s = F_s v_s, \quad (26)$$

where P_s is the nominal tire slip energy which will be used to establish the cost index of tire slip energy.

Figure 4 illustrates the simulation result of the proposed tire slip force model in the longitudinal condition. In the initial stage where the slip ratio is relatively small, the slip force is small at this time with a literally difference compared with the tire longitudinal force. But as the slip ratio increases, the slip force accounts for a larger proportion. When the tire is fully slippery, the slip force becomes equal to the tire force.

3 Problem formulation

The maximum torque of the in-wheel motor of 4WD EVs has been increasing [28], and the tire force of these EVs in the acceleration phase is continually challenging the friction limit between the tire and the ground. The energy loss in this phase mainly concentrates on the motor and the tire. The speed of the 4WD EVs in a certain acceleration period will be optimized herein to minimize the motor energy loss and the tire slip energy. The appropriate torque distribution considering the tire characteristics and the motor efficiency will make it appropriately compromise the contradictions between the motor energy loss and the tire slip energy.

Protean electric PD18 motors were used as the powertrain herein. Comparatively, the in-wheel motor can generate a high torque output, and its inverter is integrated into the motor; hence, additional power or control electronics is unnecessary. From the energy aspect, the output power of the battery will be lost in the inverter and the motor. The efficiency of the electric machine efficiency is given by a steady-state map because of the inverter integrated into the motor (Figure 5). This map is fitted as a function of both motor torque T_m and speed n_m . A corresponding power equation is used to convert the steady-state efficiency map into the motor's loss power steady-state map related to the torque T_m and speed n_m .

$$P_{\text{loss}} = \frac{P_m (1 - \eta_m)}{\eta_m}, \quad (27)$$

$$P_m = \frac{T_m n_m}{9550}, \quad (28)$$

where P_m is the instantaneous output power of the motor, P_{loss} is the instantaneous power loss of the motor, η_m is the instantaneous operating efficiency that includes the instant operating efficiency of the inverter. For analytical formulation, a simple but accurate motor power loss model needs to be developed based on the experimental data of the motor's power steady-state map. To improve the accuracy of the fitting results, the fitting area is narrowed to a specific range which is defined by motor speed (0 ~ 680 rpm) and motor torque (0 ~ 1025 Nm), according to the motor actual working area. In this paper, the motor output power loss P_{loss} is fitted as the following polynomial

$$P_{\text{loss}} = k_1 + k_2 n_m + k_3 T_m^{k_4}, \quad (29)$$

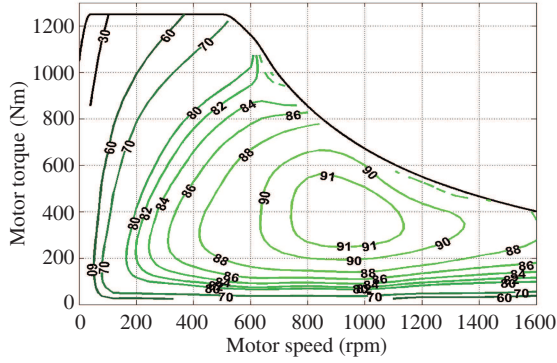


Figure 5 (Color online) In-wheel motor efficiency [23].

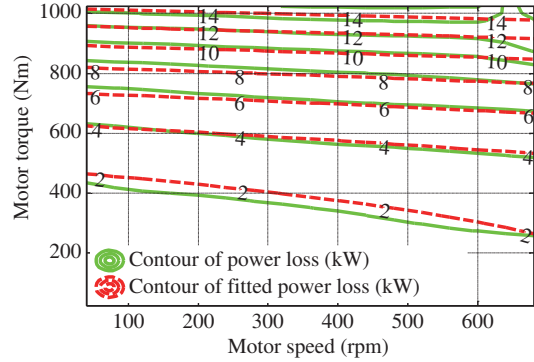


Figure 6 (Color online) Comparison of in-wheel motor power loss fitting results.

where $k_1, k_2, k_3,$ and k_4 are the fitting coefficients. The polynomial above has the minimum sum of square error compared with other fitting formulas based on the mature mathematics software 1stOpt, so this type of polynomial has the best fitting accuracy with these off-line motor data (as shown in Figure 6). The red dotted line and green line represent the contour of the fitted motor power loss data and original motor power loss data, illustrating an acceptable fitting accuracy.

The objectives of the optimal control problem formulated and solved in this paper are twofold: minimizing motor energy loss, while minimizing tire slip energy. The typical multi-objective optimization problem has various ways to solve [29], the weighted sum method is used in this case. Based on the description of the optimal condition, we propose a cost function as follows:

$$J = \int_{t_0}^{t_f} \left(\beta \frac{I_1(x(t), u(t))}{M} + (1 - \beta) \frac{I_2(x(t), u(t))}{\Lambda} \right) dt, \tag{30}$$

in which $I_1(x(t), u(t))$ represents the total motor energy loss, while $I_2(x(t), u(t))$ can be interpreted as tire slip energy. The parameter β is a weighting factor that can take any value from 0 to 1. Cost function normalization based on prior knowledge is adopted to make the two parts of the cost function numerically comparable. More specifically, we do the simulation to get the value of M when β is set as 0. On the contrast, the value of Λ can be formulated if β is set as 1.

Concretely, total motor energy loss is determined as

$$I_1(x(t), u(t)) = 2 (P_{\text{loss},r} + P_{\text{loss},f}), \tag{31}$$

where $P_{\text{loss},r}$ represents the motor power loss function of the rear in-wheel motor, and it is determined by the motor speed, $n_{m,r}$, and motor torque, $T_{m,r}$. $P_{\text{loss},f}$ represents the motor power loss function of the front in-wheel motor correspondingly.

Tire slip energy of the four wheels is determined by the slip force and slip velocity, as

$$I_2(x(t), u(t)) = 2 (F_{s,r} v_{s,r} + F_{s,f} v_{s,f}), \tag{32}$$

where $F_{s,r}, F_{s,f}$ are slip force of the rear and front tires, $v_{s,r}, v_{s,f}$ represent the slip velocity of the rear and front tires.

After introducing the construction of cost function, the discussion of constraints on optimization problems follows. According to the actual operating characteristics of the motor, inequality constraint in the optimal problem is

$$0 \leq u(t) \leq T_{m,\max} (n_m(t)), \tag{33}$$

where $T_{m,\max}$ is the peak torque of the motor, which means the physical limit of the motor. It is fitted as a piecewise function with motor speed as the independent variable.

$$T_{m,\max} (n_m(t)) = \begin{cases} 1250, & n_m(t) < 500, \\ p_1 n_m^2(t) - p_2 n_m(t) + p_3, & n_m(t) \geq 500, \end{cases} \tag{34}$$

where $p_1, p_2,$ and p_3 are fitting parameters.

To allocate the torque of the 4WD EVs in an acceleration horizon, initial and termination speeds need to be set in advance, this will serve as equality constraints in optimization problems as follow:

$$x(t_0) = v(t_0), \quad x(t_f) = v(t_f), \quad (35)$$

where $v(t_0)$, $v(t_f)$ are the initial and termination speeds.

Therefore the optimal control problem can be formulated by the following non-convex optimal problem

$$\min J = \int_{t_0}^{t_f} I(x(t), u(t)) dt \quad (36)$$

$$\begin{aligned} \text{s.t. } \dot{x}(t) &= f[x(t), u(t)], \\ \mu[x(t), u(t)] &\leq 0, \\ \gamma[x(t_f), x(t_0)] &= 0, \end{aligned} \quad (37)$$

where $x(t)$ is a state variable, in this paper, it represents the vehicle velocity v ; $u(t)$ is control variable, in this paper, it represents the motor torque of the four in-wheel motors; f is the differential equation describing the dynamic changes of the system; the inequality constraint μ can be calculated as the motor torque constraints under different motor speed (33); the terminal condition γ represents the initial speed and terminal speed (35); J is the cost function (30).

4 Solution

The formulated optimal control problem is a nonlinear optimization problem because of the nonlinear characteristic of the tire. It is discretized into N steps using the forward differential equations (FDE) in time horizon $[t_0, t_f]$,

$$\min J = \sum_{k=0}^{N+1} I[x(k), u(k)] \Delta t \quad (38)$$

$$\begin{aligned} \text{s.t. } x(k+1) &= x(k) + f[x(k), u(k)] \Delta t, \\ \mu[x(k), u(k)] &\leq 0, \\ \gamma[x(t_f), u(t_f)] &= 0. \end{aligned} \quad (39)$$

Then, the problem can be reformulated as a nonlinear programming (NLP) problem, and the purpose is changed to find the sequence of control variables and state variables $X^* = [X, U]^T \in R^{5N}$ defined by

$$\begin{aligned} X &= [v(1), v(2), \dots, v(N)], \\ U &= [T_{m,r}(1), T_{m,r}(2), \dots, T_{m,r}(N), T_{m,f}(1), T_{m,f}(2), \dots, T_{m,f}(N)] \end{aligned} \quad (40)$$

to satisfy the cost function

$$X^* = \arg \min_{u \in U} : J. \quad (41)$$

At the same time, it must satisfy the constraints of state and control variables. Consequently, this NLP problem can be solved by the interior point method (IPM) [30].

5 Simulation results

In this section, the proposed motor torque allocation algorithm is evaluated in a MATLAB environment. Table 1 presents the simulation model of 4WD EVs, which was prototyped with a full-size sports utility vehicle, and its parameters.

The other two control algorithms are also constructed as a benchmark for comparison to show the advantages of the proposed torque allocation strategy. The difference is listed as follows:

TA-AL. The wheel torque allocation based on the axle load. The misalignment of the vehicle's center of gravity and the geometric center and the load transfer caused by the acceleration will cause the difference in the vertical load between the front and rear tires. The adhesion ability of a tire is proportional to the

Table 1 Parameters of the vehicle

Symbol	Description	Value
m	Vehicle mass	2080 kg
l	Wheelbase of the vehicle	2870 mm
l_1	Distance of the front axles from the CG	1428 mm
l_2	Distance of the rear axles from the CG	1442 mm
h_g	Height of the vehicle center of gravity	498 mm
ρ	Air density	1.2258 kg/m ³
C_D	Air resistance coefficient	0.3
A	Windward area	2.58 m ²
r	Dynamic tire radius	0.36 m
μ	Rolling resistance coefficient	0.01
a	Fitting coefficient of tire longitudinal slip stiffness	-1.560109E-7
b	Fitting coefficient of tire longitudinal slip stiffness	173.226821
c	Fitting coefficient of tire longitudinal slip stiffness	0.20985322
k_s	Fitting coefficient of tire longitudinal slip stiffness	0.28
p_1	Fitting coefficient of motor torque constraints	6.616E-4
p_2	Fitting coefficient of motor torque constraints	2.158
p_3	Fitting coefficient of motor torque constraints	2177
k_1	Fitting coefficient of motor power loss	300.93
k_2	Fitting coefficient of motor power loss	1.99
k_3	Fitting coefficient of motor power loss	8.43E-5

vertical load under the same adhesion coefficient road surface. Therefore, this method is a simple, but effective method for distributing the wheel torque in proportion to the vertical force of the tire.

TA-ML. The wheel torque allocation method considering the motor energy loss in the cost function. This term is also an optimization index often used by traditional electric vehicles in economic-oriented torque optimization.

TA-SLML. The wheel torque allocation method considering the motor and tire slip energy loss.

5.1 Acceleration condition of high-adhesion coefficient road

The simulation was conducted on a high-adhesion coefficient road. The longitudinal friction coefficient was set to 0.8. The simulation scenario was configured as accelerating from 0 to 19 m/s within 4 s to simulate the rapid acceleration of 4WD EVs. Figure 7 show that TA-SLML will distribute more torque on the rear wheel at the early stage compared to TA-ML. For the front wheel, the torque distribution was opposite because if the motor loss is only the performance function of the optimal allocation method, the controller will try to work on the most efficient working point under the same motor power. The tire slip energy was considered in the TA-SLML; thus, the acceleration of the initial stage was relatively high. Moreover, the load transfer resulted in a large vertical load on the rear axle of the vehicle and a large tire longitudinal force. The existence of this potential optimization feasibility consequently resulted in the torque allocation that caused a promising optimization effect. Different from the two previous methods, the torque allocation results of TA-AL showed a slightly upward curve derived from the gradual increase of the total demand torque. This trend is attributed to the fact that the allocation strategy was based only on the axle load of the front and rear wheels. The distribution coefficient was a constant value when the acceleration was determined. However, to some extent, the tire workload was considered in this way of distribution.

Figure 8 further elaborates on some details of the allocation. The slip ratio of the front tire under TA-SLML was up to 0.1 at the beginning, but rapidly reduced to 0.05 because of the controller effect. Meanwhile, the tire slip force also reduced. However, the slip ratio of the front wheel under TA-ML is remained at approximately 0.07 for a while and resulted in the corresponding increase of the slip force and the tire slip velocity.

From the perspective of the final energy consumption in Table 2, compared with that of TA-ML, the motor energy loss of the TA-SLML grew by 1.96%, but the tire slip energy decreased by 30.06%. The motor energy loss of TA-AL was significantly larger than the others, but its tire slip energy was reduced by 10.03% compared with TA-ML, thereby verifying the slip suppression effect to a certain extent. The

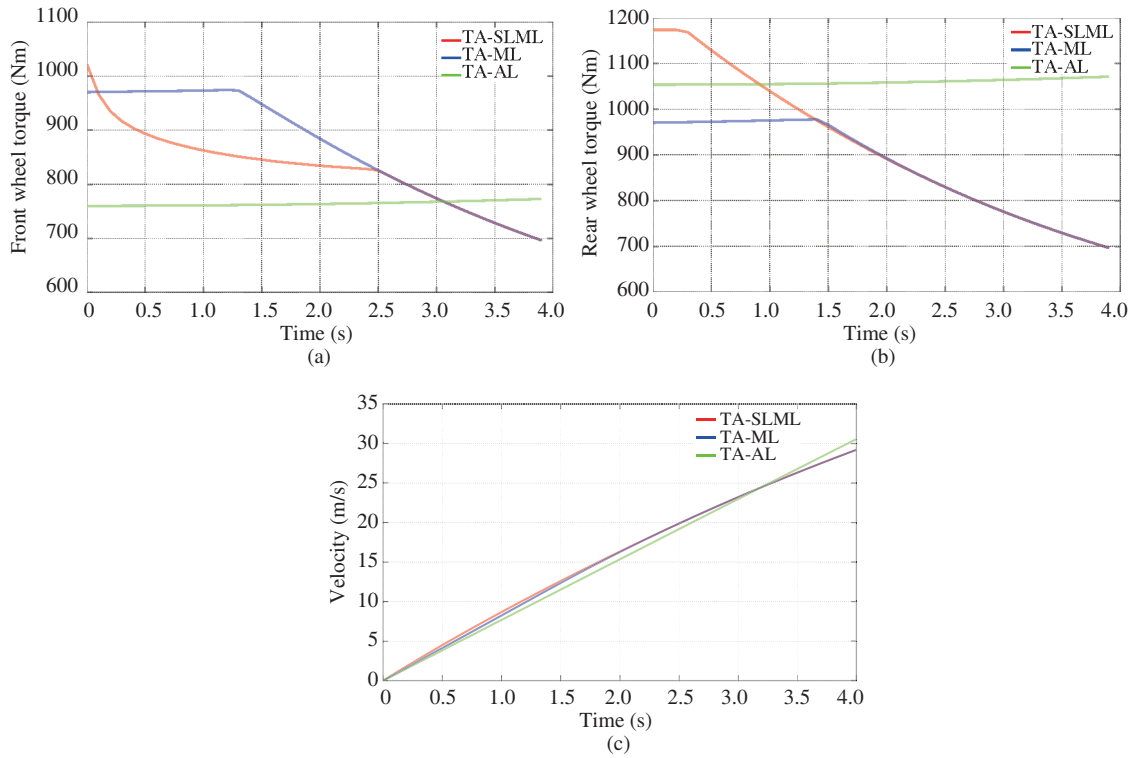


Figure 7 (Color online) Simulation results of wheel torque distribution and velocity by using three different control algorithms on the high-adhesion coefficient road. Comparison of (a) front wheel torque, (b) rear wheel torque, and (c) velocity.

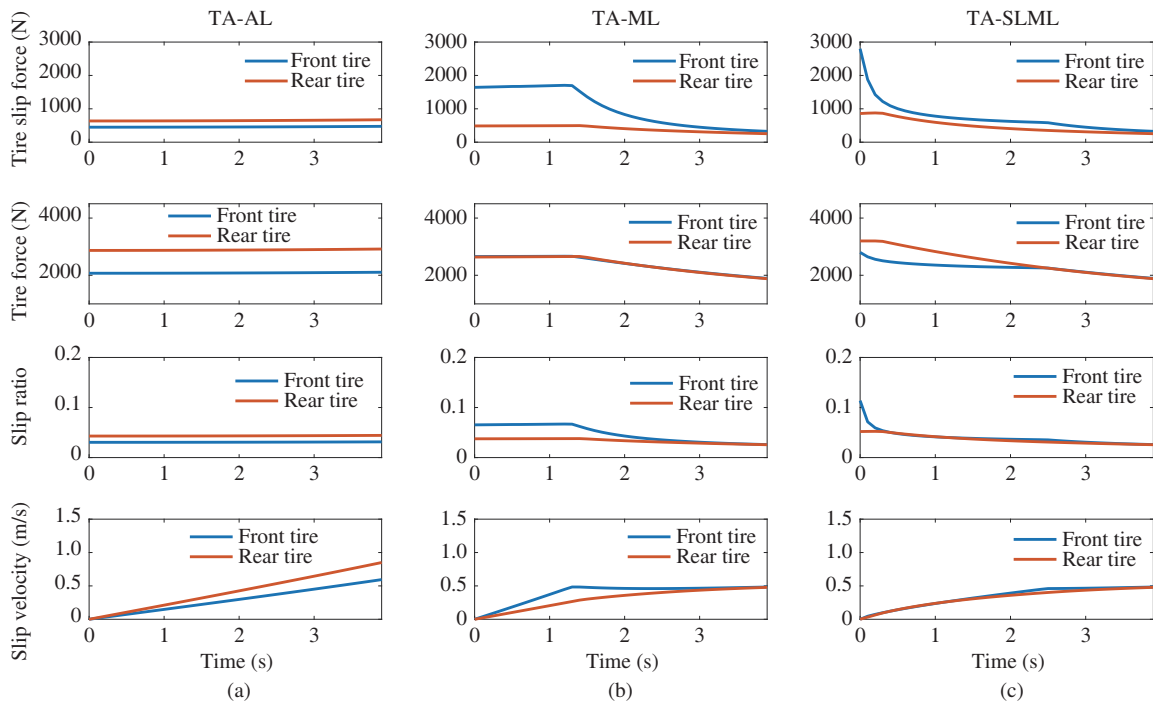
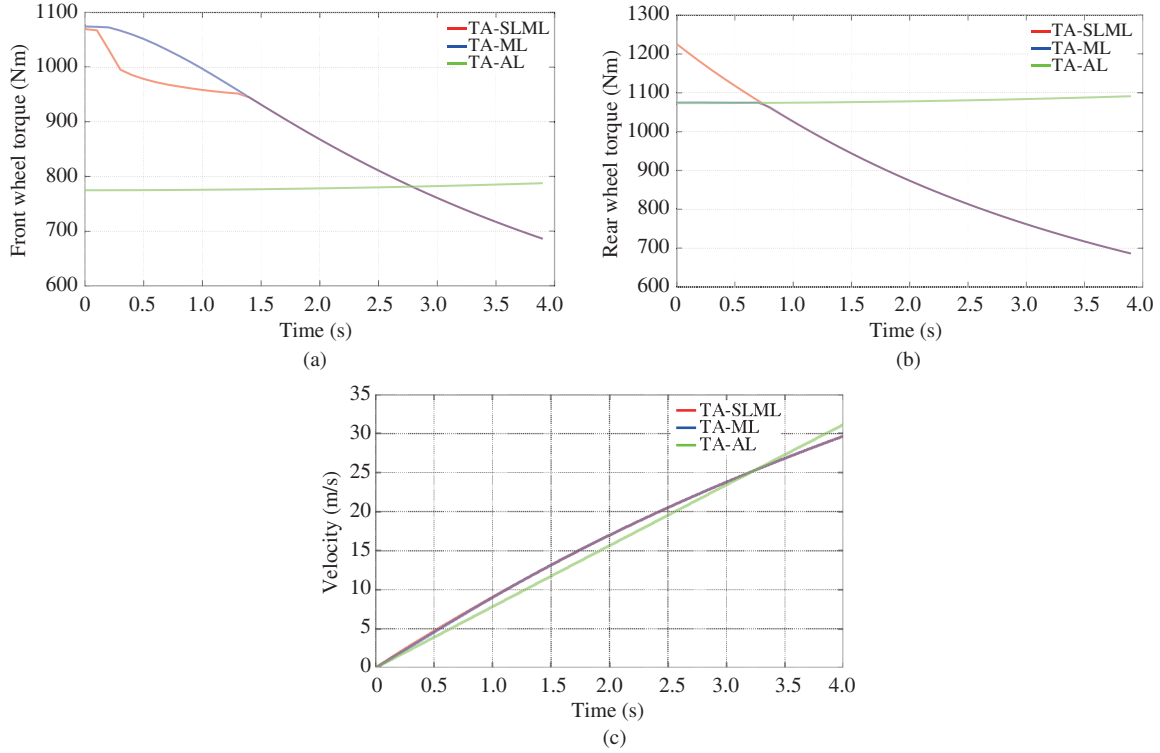


Figure 8 (Color online) Comparison of results of three different distribution control algorithms on the high-adhesion coefficient road. (a) Allocating motor torque based on axis vertical load; (b) only considering motor loss to allocate motor torque; (c) considering motor loss and slip loss both to allocate motor torque.

results showed that the TA-SLML strategy can reduce the tire slip energy and tire wear dramatically with an acceptable motor energy efficiency sacrifice.

Table 2 Energy consumption on the high adhesion coefficient road

Allocation method	Motor energy loss (J)	Tire slip energy (J)	Total energy loss (J)
TA-AL	186150	3272.6	189422.6
TA-ML	162510	3637.8	166147.8
TA-SLML	165690	2544.4	168234.4

**Figure 9** (Color online) Simulation results of wheel torque distribution and velocity by using three different control algorithms on the low-adhesion coefficient road. Comparison of (a) front wheel torque, (b) rear wheel torque, and (c) velocity.

5.2 Acceleration condition of the low-adhesion coefficient road

Another simulation condition involved acceleration on low-adhesion coefficient roads, such as slippery roads on rainy days. Thus, the longitudinal friction coefficient, μ_f , was set to 0.4. A smaller road adhesion coefficient means that the tire's driving force will always exceed the maximum adhesion force provided by the ground, and the tire will transform from a stable zone to an unstable zone more facily. In this state, more energy dissipation will transpire, and the wheel torque allocation considering the tire slip energy may be more critical. We set the simulation condition as accelerating to 18.8 m/s in 4 s.

Figure 9 depicts that the front wheel torque is larger than the rear wheel torque. The front wheel torque under TA-SLML and TA-ML were approximately 1070 Nm at the beginning; however, a sharp reduction was observed for that under TA-SLML during 1.5 s compared to that under TA-ML. The allocation result intersected with each other. Similar to the results for the high-adhesion coefficient, the allocation result of TA-AL slowly increased because of the gradual wind resistance increase. For the rear wheel, a gradual decline of the simulation results for TA-SLML was observed during the whole process, but it was still larger than that under TA-ML. Their results intersected in 0.7 s.

Figure 10(c) shows the resulting tire parameters of TA-SLML on the low adhesion coefficient road. The large acceleration at the early stage will cause severe load transfer in z axis accompanied by a higher longitudinal stiffness. The higher the longitudinal stiffness, the lower the slip rate of the tire under the same tire longitudinal force. Thus, compared with TA-ML, TA-SLML applied more motor force on the rear wheel at the beginning to avoid a significant tire slip occurrence. Figure 10(c) shows the actual effect. The slip ratio of the front tire immediately decreased to 0.06. The tire slip force and the slip velocity of the front wheel decreased as well. The tire force maintained a reasonable value to accelerate the vehicle to the set velocity at the end of the optimal horizon.

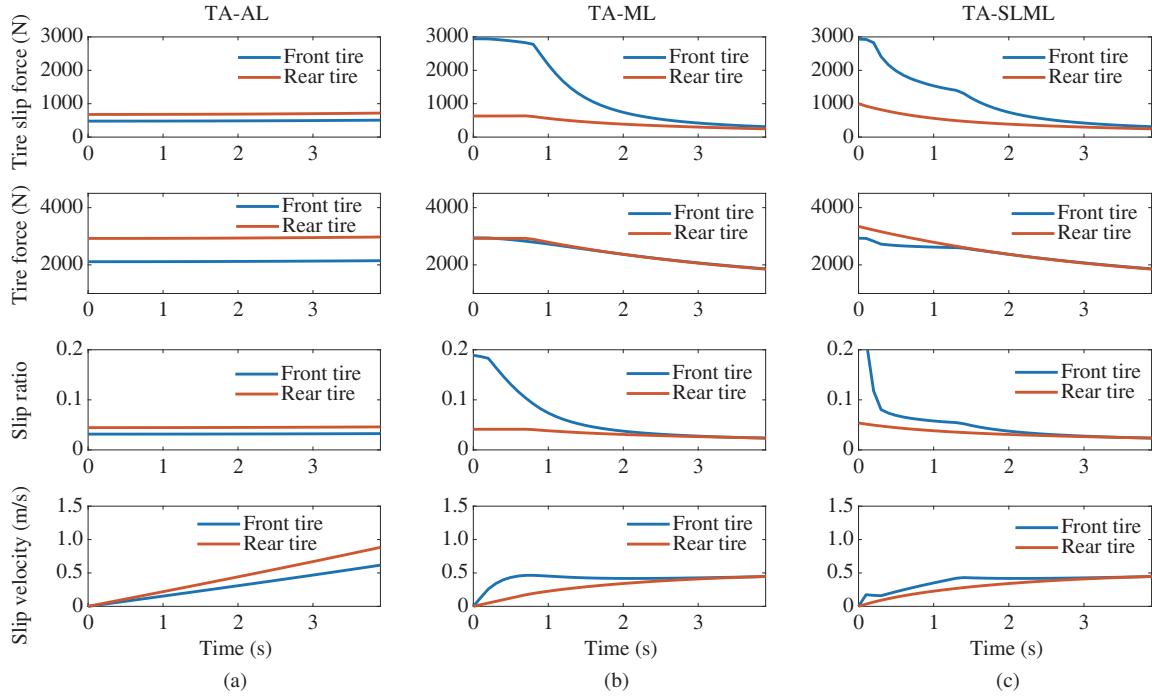


Figure 10 (Color online) Comparison of results of three different distribution control algorithms on the low-adhesion coefficient road. (a) Allocating motor torque based on axis vertical load; (b) only considering motor loss to allocate motor torque; (c) considering motor loss and slip loss both to allocate motor torque.

Table 3 Energy consumption on the low adhesion coefficient road

Allocation method	Motor energy loss (J)	Tire slip energy (J)	Total energy loss (J)
TA-AL	195320	3624.7	198944.7
TA-ML	172710	4760	177470
TA-SLML	173640	3515.7	177155.7

As a benchmark for comparison, the slip ratio of the front tire under the TA-ML control remained at approximately 0.2 for a long while in Figure 10(b). This phenomenon is unfavourable to our purpose since it will result in greater tire slip force and slip velocity.

Finally, the tire slip energy consumption and the motor loss energy consumption were compared in Table 3. TA-SLML consumed 3515.7 J tire slip energy in the whole process, while TA-ML and TA-AL consumed 4760 J and 3624.7 J, respectively. The result indicates that the proposed torque allocation algorithm can save 26.14% and 3.00% tire slip energy separately. This will prevent excessive tire slip and ensure vehicle safety in a low-adhesion coefficient road. The motor loss energy under TA-SLML was 173640 J. Although this value increases by approximately 0.54% compared with that under TA-ML, it also decreased by 11.10% compared with TA-AL. Furthermore, the total energy loss of TA-SLML was reduced by 0.18% and 10.95% separately. The algorithm proposed in this study reduced the energy consumption of the tire as much as possible while ensuring the vehicle stability.

6 Conclusion

This study presents a criterion considering both motor energy loss and tire slip energy on the torque allocation method of 4WD EVs using an optimization algorithm. We started with an energy flow analysis, illustrating a considerable percentage of the motor energy loss and tire slip energy during an acceleration condition. A semi-empirical tire slip energy model was then derived to constitute a part of the cost function. Using the proposed TA-SLML algorithm, the simulation result showed significant energy loss mitigation compared with the load and motor efficiency-based torque allocation methods, particularly on the low-adhesion coefficient road. In conclusion, the motor energy loss and tire energy indices must be considered in the torque allocation method to achieve an appropriate balance between economy and

stability. The latter index proportional to the tire wear condition can go further with the tire slip energy.

The vehicle longitudinal characteristics were considered in this paper. The future work will include research on the optimal torque allocation considering the lateral slip energy consumption in vehicle-cornering conditions. Further research could shed more light on the distributed optimization of the four-wheel torque based on the individual tire-road interface.

Acknowledgements This work was supported by National Natural Science Foundation of China (Grant Nos. 61520106008, 61790564), Jilin Provincial Science Foundation of China (Grant No. 20190103047JH), and China Automobile Industry Innovation and Development Joint Fund (Grant No. U1864206).

References

- 1 Dizqah A M, Lenzo B, Sorniotti A, et al. A fast and parametric torque distribution strategy for four-wheel-drive energy-efficient electric vehicles. *IEEE Trans Ind Electron*, 2016, 63: 4367–4376
- 2 Wang R R, Chen Y, Feng D W, et al. Development and performance characterization of an electric ground vehicle with independently actuated in-wheel motors. *J Power Sources*, 2011, 196: 3962–3971
- 3 Chen Y, Wang J M. Adaptive energy-efficient control allocation for planar motion control of over-actuated electric ground vehicles. *IEEE Trans Control Syst Technol*, 2014, 22: 1362–1373
- 4 Yuan X B, Wang J B. Torque distribution strategy for a front- and rear-wheel-driven electric vehicle. *IEEE Trans Veh Technol*, 2012, 61: 3365–3374
- 5 Pennycott A, Novellis L D, Gruber P, et al. Sources of power loss during torque-vectoring for fully electric vehicles. *Int J Veh Des*, 2015, 67: 157–177
- 6 Maeda K, Fujimoto H, Hori Y. Four-wheel driving-force distribution method for instantaneous or split slippery roads for electric vehicle. *Automatika*, 2013, 54: 103–113
- 7 Yuan L, Zhao H Y, Chen H, et al. Nonlinear MPC-based slip control for electric vehicles with vehicle safety constraints. *Mechatronics*, 2016, 38: 1–15
- 8 Xu W, Chen H, Zhao H Y, et al. Torque optimization control for electric vehicles with four in-wheel motors equipped with regenerative braking system. *Mechatronics*, 2019, 57: 95–108
- 9 Jia F J, Liu Z Y, Zhou H L, et al. A novel design of traction control based on a piecewise-linear parameter-varying technique for electric vehicles with in-wheel motors. *IEEE Trans Veh Technol*, 2018, 67: 9324–9336
- 10 Han K, Choi M, Lee B, et al. Development of a traction control system using a special type of sliding mode controller for hybrid 4WD vehicles. *IEEE Trans Veh Technol*, 2018, 67: 264–274
- 11 Zhai L, Sun T M, Wang J. Electronic stability control based on motor driving and braking torque distribution for a four in-wheel motor drive electric vehicle. *IEEE Trans Veh Technol*, 2016, 65: 4726–4739
- 12 Ahmadi J, Sedigh A K, Kabganian M. Adaptive vehicle lateral-plane motion control using optimal tire friction forces with saturation limits consideration. *IEEE Trans Veh Technol*, 2009, 58: 4098–4107
- 13 Eto R, Sakata K, Yamakawa J. Driving force distribution based on tyre energy for independent wheel-drive vehicle on rough ground. *J TerraMech*, 2018, 76: 29–38
- 14 Hu X, Wang P, Hu Y F, et al. A stability-guaranteed and energy-conserving torque distribution strategy for electric vehicles under extreme conditions. *Appl Energy*, 2020, 259: 114162
- 15 de Novellis L, Sorniotti A, Gruber P. Wheel torque distribution criteria for electric vehicles with torque-vectoring differentials. *IEEE Trans Veh Technol*, 2014, 63: 1593–1602
- 16 Zhao B, Xu N, Chen H, et al. Stability control of electric vehicles with in-wheel motors by considering tire slip energy. *Mech Syst Signal Process*, 2019, 118: 340–359
- 17 Abe M. Evaluation of active vehicle motion controls from tire energy dissipation points of view. In: *Proceedings of the 11th International Symposium on Advanced Vehicle Control*, Seoul, 2012
- 18 Suzuki Y, Kano Y, Abe M. A study on tyre force distribution controls for full drive-by-wire electric vehicle. *Vehicle Syst Dyn*, 2014, 52: 235–250
- 19 Boustani A, Sahn S, Gutowski T, et al. Tire remanufacturing and energy savings. Sloan School of Management, 2010. <http://web.mit.edu/ebm/www/Publications/MITEI-1-h-2010.pdf>
- 20 Kravchenko A, Sakno O, Lukichov A. Research of dynamics of tire wear of trucks and prognostication of their service life. *Transport Problems*, 2012, 7: 85–94
- 21 Joa E, Park K, Koh Y, et al. A tyre slip-based integrated chassis control of front/rear traction distribution and four-wheel independent brake from moderate driving to limit handling. *Vehicle Syst Dyn*, 2018, 56: 579–603
- 22 Ma Y, Chen J, Zhu X Y, et al. Lateral stability integrated with energy efficiency control for electric vehicles. *Mech Syst Signal Process*, 2019, 127: 1–15
- 23 Watts A, Vallance A, Whitehead A, et al. The technology and economics of in-wheel motors. *SAE Int J Passeng Cars-Electron Electr Syst*, 2010, 3: 37–55
- 24 Fujimoto H, Harada S. Model-based range extension control system for electric vehicles with front and rear driving-braking force distributions. *IEEE Trans Ind Electron*, 2015, 62: 3245–3254
- 25 Dugoff H. Tire Performance Characteristics Affecting Vehicle Response to Steering and Braking Control Inputs. Final Report, 1966
- 26 Pacejka H. *Tire and Vehicle Dynamics*. Amsterdam: Elsevier, 2005
- 27 Guo K H, Lu D. UniTire: unified tire model for vehicle dynamic simulation. *Vehicle Syst Dyn*, 2007, 45: 79–99
- 28 Ulrich L. Top 10 tech cars: 2018 [top 10 tech cars]. *IEEE Spectrum*, 2018, 55: 30–41
- 29 Yan L, Qu B Y, Zhu Y S, et al. Dynamic economic emission dispatch based on multi-objective pigeon-inspired optimization with double disturbance. *Sci China Inf Sci*, 2019, 62: 070210
- 30 El-Bakry A S, Tapia R A, Tsuchiya T, et al. On the formulation and theory of the Newton interior-point method for nonlinear programming. *J Optim Theory Appl*, 1996, 89: 507–541